Asian Journal of Chemistry; Vol. 28, No. 8 (2016), 1763-1769
ASIAN JOURNAL OF CHEMISTRY
http://dx.doi.org/10.14233/ajchem.2016.19816

Synthesis and Characterization of Nanocomposites Based on Styrene Butadiene Rubber/Sepiolite

FAZEELAT TAHIRA[1,*], MUNAWAR ALI[1], MUHAMMAD SHAFIQ[2] and TARIQ YASIN[2]

[1]Department of Chemistry, University of Engineering & Technology, Lahore-54890, Pakistan
[2]Department of Metallurgy and Materials Engineering, Pakistan Institute of Engineering and Applied Sciences, Islamabad, Pakistan

*Corresponding author: E-mail: fazeelat.tahira@gmail.com

Received: 4 January 2016; *Accepted*: 26 March 2016; *Published online*: 30 April 2016; AJC-17887

Styrene butadiene rubber/sepiolite nanocomposites were prepared by melt mixing of styrene butadiene rubber (SBR) with filler vinyl triethoxy silane (VTES) modified sepiolite and co-agents trimethylolpropane trimethacrylate (TMPT) and trimethylolpropane triacrylate (ATMPT). The prepared nanocomposites showed improved thermal and mechanical properties attributed to stronger cross-linking between matrix and filler compared to the control samples. The FTIR measurements confirmed grafting of trimethylolpropane trimethacrylate on SBR and development of polymer filler interactions. The SEM images revealed a good cohesion between SBR and sepiolite. The DSC analysis revealed increase in melting temperature (T_m) and crystallization temperature (T_c) with sepiolite content due to heterogeneous nucleation effect during the cold crystallization. The XRD measurements specified that the molecular frameworks of sepiolite or SBR were unaffected and modifications involved only the surface groups. In summary, investigations suggested the substantial improved properties for nanocomposites.

Keywords: Styrene butadiene rubber, Sepiolite, Nanocomposites.

INTRODUCTION

The potential of elastomer based nanocomposites has been recognized in recent years, because of their enhanced performance properties and numerous industrial applications [1,2]. The largest consumer of styrene butadiene rubber (SBR) is tyre industry, which commonly utilizes carbon black as reinforcing filler to improve wear and tear characteristics of the tyres. However, it imparts black colour to the rubber, which limits its applications for other industrial products. Moreover, production and processing of carbon black causes serious environmental problems, so there is a need to develop other reinforcing materials with improved properties for the industry and least environmental issues. Layered silicates, such as smectites, bentonite, montmorillonite and kaolinite are widely used as nano-fillers in rubber-based nanocomposites [3-6]. Recently, sepiolite, a fibrous clay mineral, has gained increasing attention as nano-filler for polymeric substances due to its high surface area and grafting properties [7]. It is a natural phyllosilicate composed of tetrahedral layers of SiO_4 sandwiched between octahedral sheet of magnesium hydroxides with unit cell formula $[Si_{12}O_{30}Mg_8(OH)_4](H_2O)_4{\cdot}8H_2O$. It morphology is needle like (2-10 μm long, 100-300 nm wide) with internal structural channels of cross section (11 × 4 $Å^2$) that are associated with zeolitic water [8-10; Fig. 1]. Sepiolite contains significant number of silanol (Si–OH) groups, which can be functionalized to achieve satisfactory dispersion and performance properties of nanocomposites [11-15].

In this study, we have prepared nanocomposites by modifying both polymer matrix SBR and nano-filler sepiolite (Table-1). The former represents a low polarity polymer matrix while latter is a hydrophilic clay hence an interpenetration link between the two cannot be developed; therefore, SBR was modified by tri-functional monomers: trimethylolpropane trimethacrylate (TMPT) and trimethylolpropane triacrylate (ATMPT), while sepiolite was modified by vinyl triethoxy silane (VTES) coupling with main objective to create covalent linkages on their surfaces as suggested previously [16-18]. The zeolitic water or hydroxyl groups present in the octahedral magnesium layers offer favourable sites for the attachment of organic molecule onto the inorganic framework, *via* organosilane grafting. Following the grafting, the original hydrophilic surface of sepiolite becomes organophilic, which in turn enhances the compatibility between SBR and modified sepiolite [19-21].

EXPERIMENTAL

Styrene butadiene rubber (density: 0.926 g/mL; melting point: 123 °C) was purchased from Exxon Mobil chemical (Riyadh, Saudi Arabia), VTES: (density: 0.901 g/mL; mole-

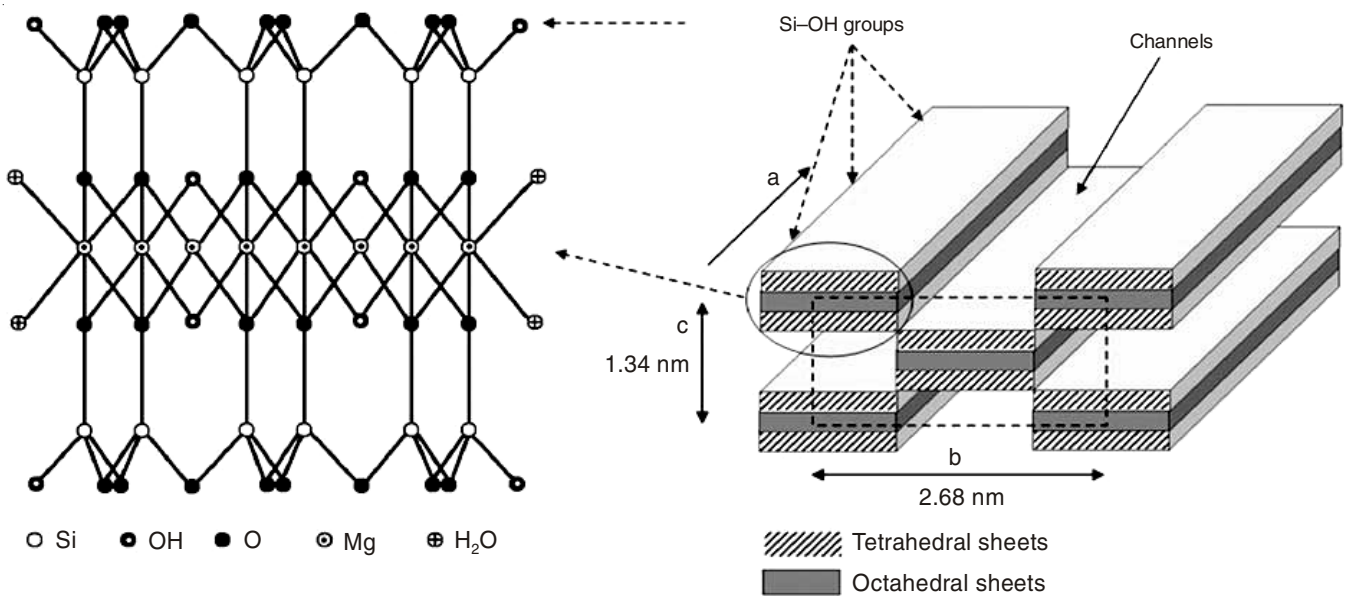

Fig. 1. Crystalline structure of sepiolite [27,28] Fibre structure of sepiolite [29]

cular weight: 190), stearic acid (density: 0.926 g/mL; molecular weight: 284.48) and sepiolite ($Mg_4Si_6O_{15}(OH)_2.6H_2O$; surface area: 300 m^2/g; molecular weight: 646) were purchased from Sigma-Aldrich Chemie, (Steinheim, Germany). Other chemicals *e.g.*, zinc oxide, sulfur, paraffin oil, antioxidant, TMPT ($C_{18}H_{26}O_6$; density: 1.06 g/mL; formula weight: 338), ATMPT ($C_{15}H_{20}O_6$; density: 1.1 g/mL; formula weight: 296), polyethylene wax, 2-bisbenzothiazole-2,2′-monosulfide (MBTM; $C_{14}H_8N_2S_3$, cross linking initiator) and 2-bisbenzothiazole-2,2′-disulfide (MBTS; $C_{14}H_8N_2S_4$, cross linking accelerator) were purchased from local suppliers (Sigma-Aldrich) and were analytical grade.

The VTES modified sepiolite (MS) was prepared according to published method [21,22]. For the preparation of SBR base material, zinc oxide (5 phr), stearic acid (1 phr), antioxidant (1 phr) and polyethylene wax (5 phr) were mixed with SBR (100 g) using roller rotter for 20 min at speed 60 rpm at 90 °C. In second stage mixing was done for 15 min. at 60 rpm, 120 °C utilizing banbury rotors. SBR base material thus obtained was used to prepare different formulations. The codes and compositions of nanocomposites are shown in Table-1.

The control formulations, CS, CS_1, CS_3 and CS_5 were prepared by *in situ* copolymerization of SBR with modified sepolite (0, 1, 3 and 5 phr) at 120 °C in internal mixer at 60 rpm for 15 min utilizing banbury rotors; control sample (CS) represents neat SBR used for comparison purposes.

Trifunctional monomer formulations, TMS_1, TMS_3 and TMS_5, were prepared by blending SBR (100 g) with modified

TABLE-1
CODES AND COMPOSITION OF CONTROL AND OTHER TRIFUCNTIONAL MONOMER FORMULATIONS

Sample code	Amount (phr)													
	SBR	SP	VTES	MS	ZnO	Anti-oxidant	Poly ethylene wax	Stearic acid	Paraffin oil	TMPT	ATMPT	S	MBTS	MBTM
Control														
CS	100	0	0	0	5	1	5	1	0	0	0	0	0	0
CS_1	100	0	0	1	5	1	5	1	7	0	0	0	0	0
CS_3	100	0	0	3	5	1	5	1	7	0	0	0	0	0
CS_5	100	0	0	5	5	1	5	1	7	0	0	0	0	0
Polyfucntional monomer formulations														
*TMS_1	100	1	0	0	0	0	0	0	0	0	0	0	0	0
*TMS_3	100	3	0	0	0	0	0	0	0	0	0	0	0	0
TMS_1	100	0	0	1	5	1	5	1	0	3.38	0	0	0	0
TMS_3	100	0	0	3	5	1	5	1	0	3.38	0	0	0	0
TMS_5	100	0	0	5	5	1	5	1	0	3.38	0	0	0	0
$ATMS_1$	100	0	0	1	5	1	5	1	0	0	2.96	0	0	0
$ATMS_3$	100	0	0	3	5	1	5	1	0	0	2.96	0	0	0
$ATMS_5$	100	0	0	5	5	1	5	1	0	0	2.96	0	0	0
Sulfur cross-linked formulations														
MBT_1	100	0	0	1	5	1	5	1	0	0	0	2	1	1
MBT_3	100	0	0	3	5	1	5	1	0	0	0	2	1	1
MBT_5	100	0	0	5	5	1	5	1	0	0	0	2	1	1

Note: refer to section for definition of abbreviations; *Unmodified sepiolite was used in these formulations; phr = parts per hundred of rubber

sepiolite (1, 3 and 5 phr) followed by addition of TMPT (10 mmol or 3.38 phr) in all formulations. Mixing was done at 120 °C at 60 rpm for 15 min using banbury rotors. In formulations *TMS_1, *TMS_3 (Table-1) sepiolite without modification was used. Similarly formulations $ATMS_1$, $ATMS_3$ and $ATMS_5$ were prepared following the above mentioned procedure however ATMPT (10 mmol or 2.96 phr) was used instead of TMPT.

Cross-linked sulfur formulations, MBT_1, MBT_3 and MBT_5, were prepared as per ASTM D 3182 and 3184 [23,24]. Briefly, SBR (100 g) was mixed with modified sepiolite (1, 3 and 5 phr) followed by addition of cross-linking initiator MBTM (1 phr). The contents were cooled to room temperature before the addition of accelerator MBTS (1 phr) and elemental sulfur (2 phr), was added. The operating conditions of internal mixer were the same as that of trifunctional monomer formulations.

The formulations prepared above were molded to sheet by hydraulic press (Gibitre Hot press) at 150 MPa and 100 °C. The sheets were packed in air free polyethylene bags and sent for radiations treatment at Pakistan Radiation Services, Pakistan Atomic Energy Commission, Pakistan. The molded sheets were irradiated using an accelerator ALIN-10 for 15-20 days. The accelerated electrons dose was 2.4 kGy/min in order to accumulate 2.5 Mrad, 5 Mrad, 7.5 Mrad and 10 Mrad respectively (1 Mrad = 10 kGy).

Analysis: The mechanical properties were determined on a 'Zwick' universal testing machine (mode1 1445) at a crosshead speed of 500 mm/min as per ASTM D 412-06 A [25]. Dumbbell specimens were punched out of the molded sheet using a die. The sample was held tight by the two grips at 28 ± 2 °C and subjected to uniaxial tensile force which is continuously increasing. The readings of tensile strength, elongation at break (E_b) and tensile modulus, M100 (stress at 100 % elongation) were recorded by the microprocessor.

The hardness was determined using a Shore Durometer type D Reed Hardness Tester (model RR12) according to ASTM D D2240-05 [26]. The samples (30 mm dia and 1 mm thickness) were subjected to load of 12.5 N. The readings were taken after 10 seconds of indentation.

The procedures for Fourier transform infrared (FTIR) analysis, thermal gravimetric analysis (TGA), X-ray diffraction (XRD), scanning electron microscopy (SEM) and differential scanning calorimetry (DSC) have been described in earlier publications [21,22].

RESULTS AND DISCUSSION

Mechanical properties: The mechanical properties, such as, ultimate tensile strength (UTS), Young's modulus (E), elongation at break (E_b), stress at break (σ_b) and yield stress (σ_y) of neat SBR and its composites are summarized in Table-2, while stress-strain curves are shown in Fig. 2. Ultimate tensile strength of sepolite filled nanocomposites is slightly higher than that of control sample (CS). The formulations with modified or unmodified sepolite and co-agents, *e.g.* TMS_1, TMS_3, $ATMS_1$ and $ATMS_3$ show almost same ultimate tensile strength. There is no change in ultimate tensile strength at low filler concentration.

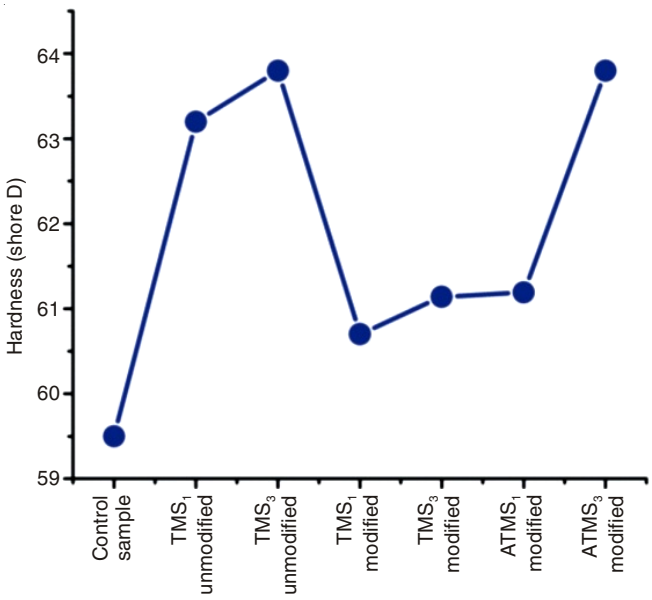

Fig. 2. Hardness (shore D) of neat SBR and its nanocomposites

Young's modulus of nanocomposites filled with modified and unmodified sepiolite increases remarkably up to 352.3 MPa and 377 MPa for TMS_3 and TMS_3 (unmodified) respectively compared to control sample (268.5 MPa). The nanocomposites with 3 phr sepiolite show the highest modulus within a given formulation set suggesting increase in modulus with clay content. The increase in modulus even at small sepiolite concentration may be linked to the higher degree of filler dispersion and increased interaction between filler and SBR. The possible reason why Young's modulus is less for modified sepiolite nanocomposites might be that the VTES forms a lubricative interface between filler and SBR chains, thus causing stress relaxation.

The elongation at break decreases drastically-observed values for TMS_1 & TMS_3 unmodified, TMS_1, TMS_3, $ATMS_1$ and $ATMS_3$ are: 10.1 %, 10.3 %, 16 %, 22.2 %, 7.5 % and 8.2 % respectively while same parameter for control sample

TABLE-2
TENSILE PROPERTIES OF NEAT SBR AND NANOCOMPOSITES

Properties	CS	*TMS_1	*TMS_3	TMS_1	TMS_3	$ATMS_1$	$ATMS_3$
UTS (MPa)	13.2 ± 0.4	13.8 ± 0.3	13.5 ± 0.3	12.8 ± 0.4	13.3 ± 0.5	13.4 ± 0.2	13.3 ± 0.1
E (MPa)	268.5 ± 3.8	320.0 ± 3.7	377.0 ± 4.6	225.4 ± 1.2	242.0 ± 3.6	343.9 ± 17	352.3 ± 2.7
E_b (%)	105.1 ± 1.3	10.1 ± 1.2	10.3 ± 1.0	16.0. ± 0.7	22.2 ± 1.3	7.5 ± 1.0	8.2 ± 0.5
σ_b (MPa)	4.8 ± 0.7	8.0 ± 0.8	7.6 ± 0.8	2.80 ± 0.7	7.0 ± 0.9	5.0 ± 0.5	7.9 ± 0.5
σ_y (Mpa)	10.1 ± 0.2	8.0 ± 0.3	5.5 ± 0.4	3.7 ± 0.4	6.7 ± 0.3	5.8 ± 0.6	8.5 ± 0.5

*Formulations prepared with unmodified sepiolite; ultimate tensile strength (UTS); Young's modulus (E); elongation at break (E_b); stress at break (σ_b) and yield stress (σ_y)

is 105.1 %. This decrease may be ascribed to filler particles, which restricts the motion of SBR and decrease E_b. These data suggest a strong cross-linking between matrix and filler. More cross-linking occurs upon irradiation. Stress at break (σ_b) generally improves up to 8 MPa, 7 MPa and 7.9 MPa for *TMS_1, TMS_3 and $ATMS_3$ respectively compared to control sample (4.8 MPa) suggesting that prepared materials can withstand more stress/load compared to control.

The hardness of nanocomposites increases with clay content compare to neat polymer (control sample; Fig. 2), TMS_3 and $ATMS_3$ with 3 phr of sepiolite are the hardest among the samples suite. The improvement in hardness of nanocomposites is attributed to high interfacial interaction between the filler and SBR, high cross-linking density and reduced resilience of the SBR with the addition of clay filler. The hardness seams to follow Young's modulus (Table-2), which demonstrates that the improvement in hardness of the filled nanocomposites is caused by an increase in the cross-link density.

The mechanical properties like UTS, E, E_b and σ_b of the nanocomposites have shown significant improvement. The nanocomposites containing 1 and 3 phr of modified sepiolite and 10 mmol of co-agents TMPT and ATMPT have shown higher physical-mechanical characteristics than that of the control samples. The study proves enhanced mechanical properties of nanocomposites prepared from low cost materials and potential for new industrial applications.

Fourier-transform infrared spectrometry: The FTIR spectra of VTES modified sepiolite, control sample of neat SBR and its nanocomposites filled with modified sepiolite (1, 3 and 5 phr) and co-agent TMPT (3.38 phr) are shown in Fig. 3. In spectrum of modified sepiolite, low intensity bands in the region 3700-3300 cm^{-1} are ascribed to utilization of O–H of octahedral sheet of sepiolite in bond formation with VTES [27]. Broad bands in the region 3370-3200 cm^{-1} are due to H–O–H vibrations of zeolitic water (Fig. 3A). The absorption bands at 500 cm^{-1} are mainly assigned to Si–O bonds in the tetrahedral sheet. The wide band centered at 974 cm^{-1} is due to Si–O–Si linkages. The reduced absorption bands at 787and 694, 644 cm^{-1} are ascribed to O–H deformation and bending vibrations, respectively [28].

In Fig. 3B dominant peaks in spectrum of control sample (neat SBR) are CH_2 scissoring at 1449 cm^{-1}, bands at 2916 and 2844 cm^{-1} due to C–H methylene stretches. Other significant peaks related to the aromatic ring are at 1495 and 1452 cm^{-1} and peak at 650 cm^{-1} is due to C–H out of plane (oop) bending. The prominent band at 697 cm^{-1} is due to C–H absorption of styrene. The nanocomposites (TMS_1, TMS_3 and TMS_5) exhibit all the above mentioned C–H stretching and bending peaks; plus bands at 1020 and 1080 cm^{-1} which are attributed to the presence of siloxane-linkages. It is noteworthy that a broad band in the range of 1660-1570 cm^{-1} characteristic of carbonyl groups of , α,β-unsaturated ester, is observed in the nanocomposites, which suggest grafting of TMPT on polymer matrix. The IR spectra revealed the polymer filler interactions and co-agent linkages have been developed.

Scanning electron microscopy: Dispersion status of filler and polymer matrix was examined by SEM. Fig. 4 shows the SEM images of fractured surface of TMS_3 at various magnifications. Figs. 4A and 4B exhibit the homogeneous distribution and dispersion of nano-sized polymer-coated sepiolite particles. The existence of diffused boundaries in high magnification image indicates good compatibility between SBR and filler. The good adhesion between the two is attributed to co-agents.

X-ray diffraction analysis: The X-ray diffraction patterns of sepiolite, modified sepiolite, control sample of neat SBR and its nanocomposites: TMS_1 and TMS_3 with 1 and 3 phr of modified sepiolite and 3.38 phr TMPT are presented in Fig. 5. The sepiolite displays an intense peak at 2θ = 7.27° (d-spacing 1.22 nm) which is a typical (110) peak representing internal channel reflection of sepiolite [19]. The diffraction peak at 2θ = 26.75° (d-spacing 0.33 nm) is also observed in XRD pattern of sepiolite. The same peaks are observed in XRD pattern of modified sepiolite. This indicates that the molecular framework of sepiolite is unaffected during modification and modification involves only the surface hydroxyl groups. Fig. 5B displays the XRD pattern of neat SBR (control sample) and nanocomposites TMS_1 and TMS_3. The strong diffraction peaks at 2θ = 21.5° (d-

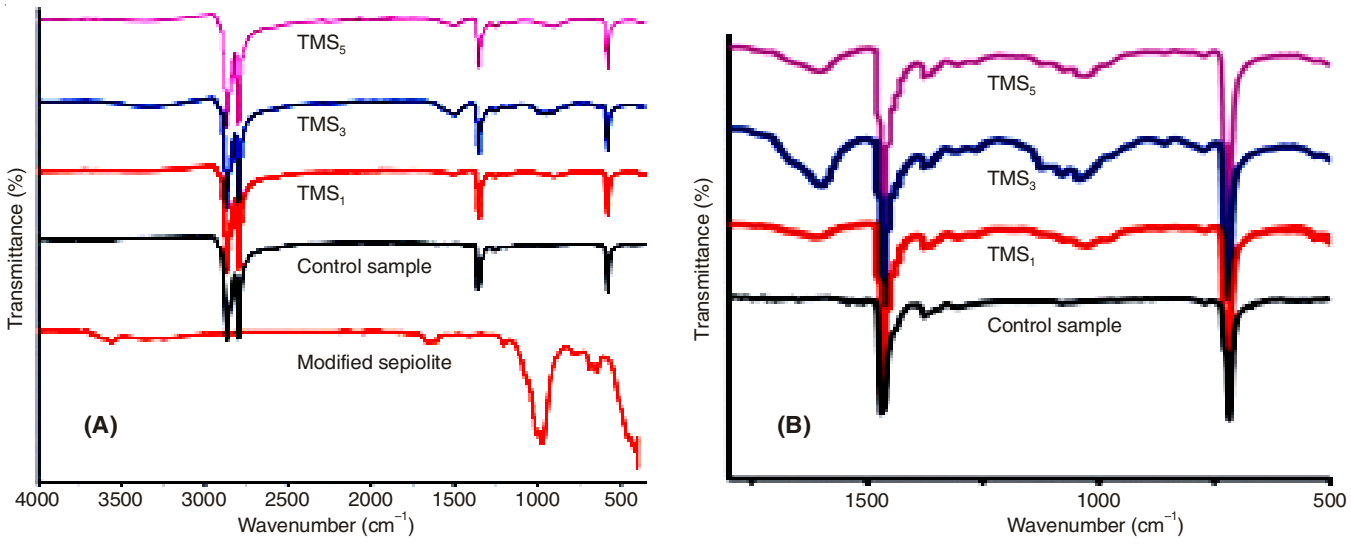

Fig. 3. FT-IR spectra showing major absorption band in samples: VTES modified sepiolite (MS), control sample (CS) and nanocomposites TMS_1, TMS_3 and TMS_5, containing 1,3 and 5 phr of modified sepiolite and 3.38 phr TMPT (trimethylol propane triacrylate)

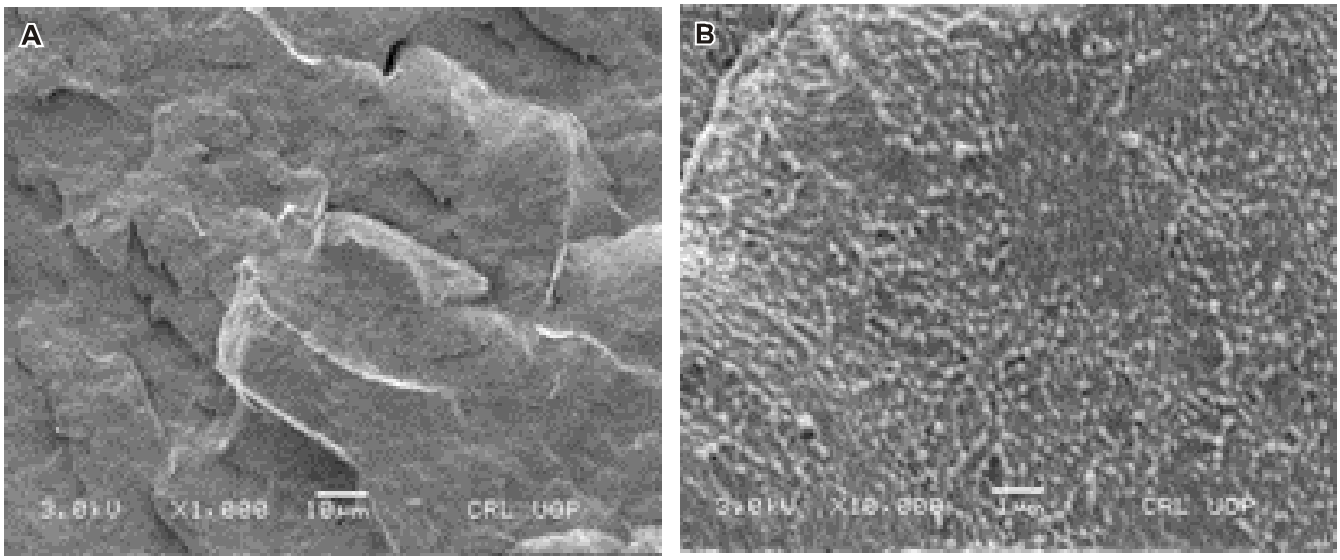

Fig. 4. SEM images of nanocomposite TMS_3 at various magnifications

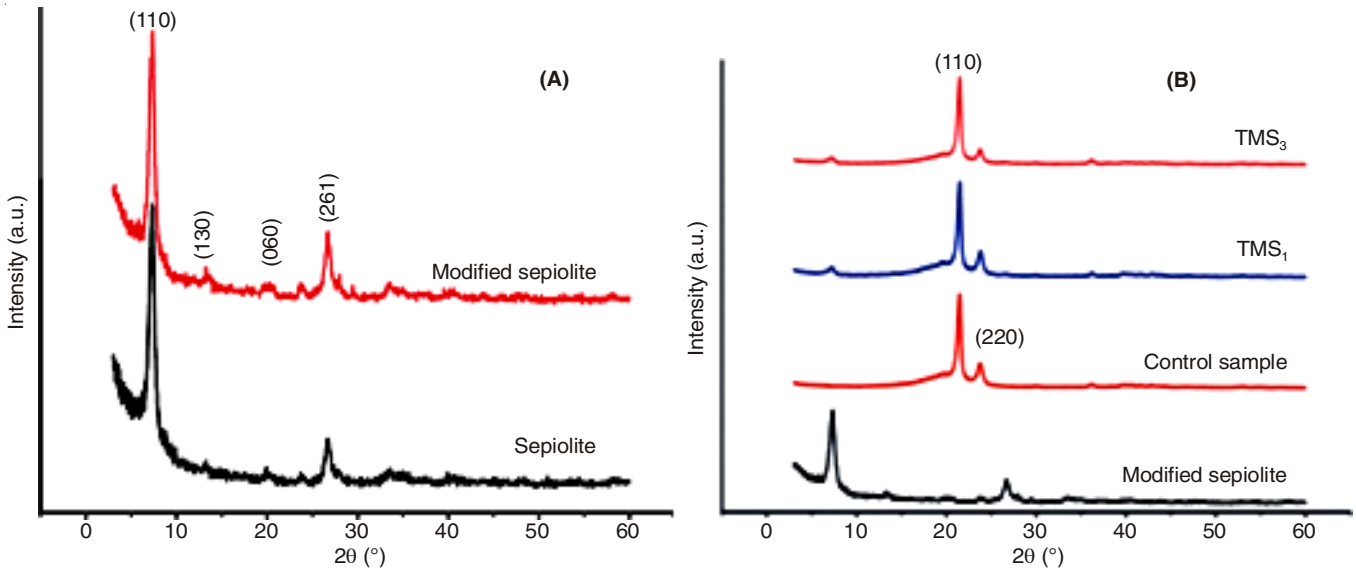

Fig. 5. XRD of pattern of sepiolite and modified sepiolite (A) control samples of neat SBR and its nanocomposites, TMS_1 and TMS_3 with 1 and 3 phr of modified sepiolite and 3.38 phr TMPT(B)

spacing 0.41 nm) and 2θ = 23.7° (d-spacing 0.37 nm) are attributed to (110) and (220) crystallographic planes of SBR and represent orthorhombic unit cell. In nanocomposites, the diffraction peaks of sepiolite have reduced in intensity at 7.27° due to small amount of filler as suggested previously [21,29-31].

Thermogravimetric analysis: The thermal stabilities of pure SBR and SBR-sepiolite nanocomposites were exploited by thermogravimetric analysis. Fig. 6 shows the thermograms of modified and unmodified sepiolite (A) and neat SBR and its nanocomposites (B) and data is summarized in Table-3. The sepiolite undergoes step-wise weight loss with increasing temperature. The first weight loss of 8.5 % is due to all types of adsorbed water, which is completed up to 170 °C. Another weight loss in the range 300-350 °C is due zeolitic water associated with the internal structure of sepiolite. The total weight loss of 14.9 % is observed up to 800 °C. The TGA curve of modified sepiolite shows weight loss around 15 %,

TABLE-3
THERMOGRAVIMETRIC ANALYSIS OF NEAT SBR AND NANOCOMPOSITES

Sample code	$T_{10\,\%}$ (°C)	$T_{50\,\%}$ (°C)	$T_{90\,\%}$ (°C)	$T_p^{(a)}$ (°C)	Residue (%) 550 °C
CS	472.9	485.9	500.4	490.0	2.3
TMS_1	474.4	487.0	502.4	490.1	3.7
TMS_3	470.1	490.9	506.2	493.8	4.0
TMS_3 unmodified	475.6	491.5	503.6	492.0	3.0

[(a)]Peak temperature of mass loss.

but not in steps similar to sepiolite, which might be due to the presence of organic moiety in modified sepiolite.

It is demonstrated in Fig. 6 that nanocomposites exhibit greater thermal stability than neat SBR, which could be due to crosslinking which gives high tensile strength to nanocompo sites, hence thermal stability is increased. Nanocomposites containing sepiolite (Table-3) have high thermal stability than

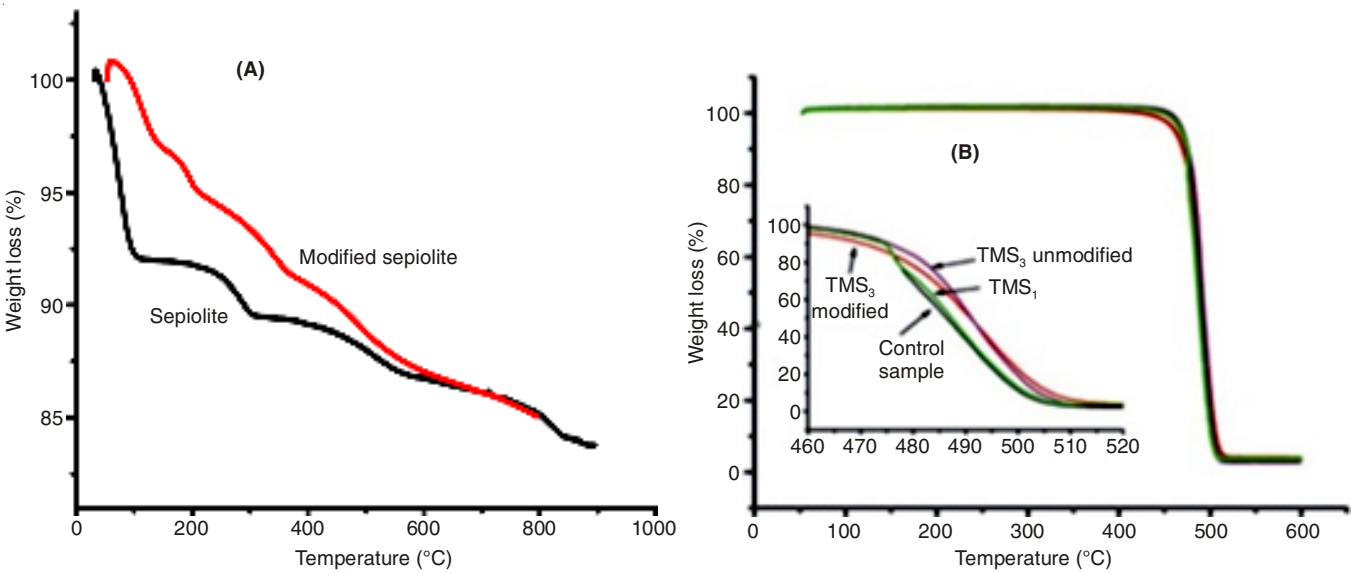

Fig. 6. TGA curves of sepiolite and modified sepiolite (A) and neat SBR (CS) and its nanocomposites TMS_1, TMS_3 modified and TMS_3 unmodified (B). Refer to Table-1 for samples details

SBR. A delay of 5.6 °C in the 50 % weight loss of TMS_3 unmodified compared to neat SBR shows the higher thermal stability resulted from the addition of sepiolite in polymer matrix. Additionally, an increase of 5.8 °C in 90 % weight loss of modified sepiolite nanocomposite (TMS_3) compared to neat SBR further confirms the higher thermal stability caused by sepiolite. Furthermore, TMS_3 modified shows higher thermal stability than TMS_1 above 10 % weight loss. The possible reason for this behaviour might be that the nano-sized sepiolite particles develop chemical bonds with VTES-grafted SBR chains through their OH groups *via* condensation reactions. Nanocomposite TMS_1 exhibits higher thermal stability than SBR. Table-3 shows that char yield (carbon or carbonaceous material left at the highest temperature of TGA analysis) is enhanced with sepiolite contents, which is attributed to heat resistant properties of sepiolite. As expected, the residual mass after pyrolysis increases with the filler content. The maximum degradation temperature of TMS_3 unmodified and TMS_3 modified is higher than pure SBR due to high thermal stability of former. Increased thermal stability of nanocomposites is ascribed to the ability of sepiolite to form a protective inorganic layer at the surface of polymer compared to SBR. Both the powerful interactions and the defensive layer formation marginal increase in thermal stability perceive for the nanocomposites. The results of thermogravimetric analysis reveal that thermal stability of nanocomposites TMS_1, TMS_3 modified and TMS_3 unmodified is apparently improved in comparison with the control sample.

Differential scanning calorimetric analysis: Differential scanning calorimetry curves of control sample and nanocomposites TMS_1, TMS_3 and TMS_3 unmodified are shown in Fig. 7. The values of melting temperature (T_m), crystallization temperature (T_c) and per cent crystallinity (X_c) are presented in the Table-4. The heating curves demonstrate that control sample exhibits T_m: 123.8 °C, the value increases up to maximum 126.2 °C with incorporation of 1 phr modified sepiolite (TMS_1; Fig. 7B; Table-4); for TMS_3 (3 phr modified sepiolite) and TMS_3 unmodified (3 phr sepiolite) increase is up to 125.6 °C and 124.9 °C respectively. Cooling curves display that T_c of TMS_1 and TMS_3 unmodified has shifted to higher temperature,

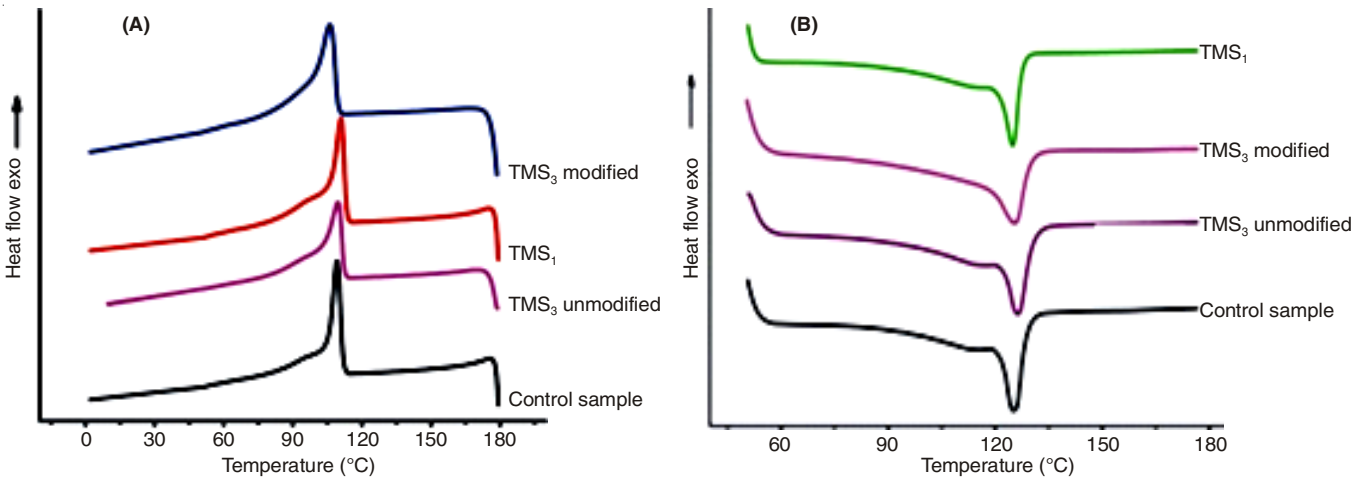

Fig. 7. DSC curves of SBR and SBR/sepiolite nanocomposites, cooling curves (A) and heating curves (B)

i.e., an increase in T_c of 0.7 °C is observed for TMS_1 and 1.7 °C for TMS_3 unmodified, although, TMS_3 shows a decrease in T_c compared to control sample (Fig. 7A; Table-4). The inclusion of the sepiolite may have induced heterogeneous nucleation during the cold crystallization process and increased the crystallinity of the nanocomposites.

TABLE-4
MELTING AND CRYSTALLIZATION CHARACTERISTICS OF NANOCOMPOSITES

Sample code	T_m (°C)	T_c (°C)	X_m (%)
CS	123.8	109.2	16.2
TMS_1	126.2	110.0	13.5
TMS_3	125.6	106.1	15.3
TMS_3 unmodified	124.9	110.9	14.7

Conclusion

Nanocomposites composed of base material SBR, VTES modified sepiolite as filler and co-agents TMPT and ATMPT, exhibited improved mechanical properties and enhanced thermal stability. The FTIR measurements confirmed grafting of TMPT on SBR and development of polymer filler interactions. The SEM images showed good cohesion between SBR and filler. Differential scanning calorimetry results revealed an increase in T_m and T_c with sepiolite content. The XRD measurements indicated that interactions involved only the surface groups while molecular framework of sepiolite and SBR was unaffected.

REFERENCES

1. P.C. Meneghett, Ph.D. Thesis, Synthesis and Properties of Rubber–Clay Nanocomposites, Case Western Reserve University, Cleveland, USA (2005).
2. L. Zhang, Y. Wang, Y. Wang, Y. Sui and D. Yu, *J. Appl. Polym. Sci.*, **78**, 1873 (2000).
3. J. Ma, J. Xu, J.H. Ren, Z.Z. Yu and Y.W. Mai, *Polym.*, **44**, 4619 (2003).
4. K.S. Maya, Ph.D. Thesis, Studies on *in situ* Precipitated Silica Filled Rubber Composites, Cochin University of Science and Technology, Cochin, India (2007).
5. L.E. Yahaya, K.O. Adebowale, A.R.R. Menon and B.I. Olu-Owolabi, *Am. J. Mater. Sci.*, **2**, 1 (2012).
6. L.B. de Paiva, A.R. Morales and F.R. Valenzuela Díaz, *Appl. Clay Sci.*, **42**, 8 (2008).
7. Y. Zheng, Y. Zheng, *J. Appl. Polym. Sci.*, **99**, 2163 (2006).
8. D.M. Moore and R.C. Reynolds, X-Ray Diffraction and the Identification and Analysis of Clay Minerals, Oxford University Press, New York, edn 2, p. 378 (1997).
9. M. Alvarado, R.C. Chianelli and R.M. Arrowood, *Bioinorg. Chem. Appl.*, **2012**, 1 (2012).
10. K. Brauner and A. Preisinger, *Tsch. Miner. Petr. Mitt.*, **6**, 120 (1956).
11. M. Galimberti, V. Cipolletti and S. Giudice, In Rubber Clay Nanocomposites Science, Technology and Applications, Chapter 7, In: Morphology of Rubber Clay Nanocomposites, Wiley & Sons, New York, p. 181 (2011).
12. Y.P. Wu, Y. Ma, Y.Q. Wang and L.Q. Zhang, *Macromol. Mater. Eng.*, **289**, 890 (2004).
13. S.K. Kim, J.-H. Kang, Y. Choe and Y.-W. Chang, *Macromol. Res.*, **14**, 187 (2006).
14. J. Wang and D. Chen, *J. Nanomater.*, **2013**, 11 (2013).
15. L. Bokobza, A. Burr, G. Garnaud, M.Y. Perrin and S. Pagnotta, *Polym. Int.*, **53**, 1060 (2004).
16. J.K. Duan, C. Kim and P.K. Jiang, *Polym. Compos.*, **31**, 347 (2010).
17. J.K. Duan, C. Kim and P.K. Jiang, *J. Polym. Res.*, **16**, 45 (2009).
18. A. Chandra, S. Gong, M. Yuan, L.-S. Turng, P. Gramann and H. Cordes, *Polym. Eng. Sci.*, **45**, 52 (2005).
19. F. Bergaya, B. Theng and G. Lagaly, Handbook of Clay Science, Elsevier, Amsterdam, p. 1224 (2006).
20. N. Herrera, J.M. Letoffe, J.L. Putaux, L. David and B.L. Elodie, *Langmuir*, **20**, 1564 (2004).
21. M. Shafiq, T. Yasin and S. Saeed, *J. Appl. Polym. Sci.*, **123**, 1718 (2012).
22. I. Ahmad, M. Shafiq and T. Yasin, *J. Appl. Polym. Sci.*, **128**, 2236 (2013).
23. ASTM D3182–07, Standard Practice for Rubber–Materials, Equipments and Procedures for Mixing Standard Compounds and Preparing Standard Vulcanized Sheets, 09.01 (2012).
24. ASTM D3184, Standard Practice for Rubber-Evaluation of NR (Natural Rubber), 09.01 (2011).
25. ASTM D412–06a, Standard Test Methods for Vulcanized Rubber and Thermoplastic Elastomers–Tension, 09.01 (2013).
26. ASTM D2240 –05, Standard Test Method for Rubber Property–Durometer Hardness, 09.01 (2010).
27 J.D. Russell, in ed.: M.J. Wilson, Infrared Methods, In: Handbook of Determinative Methods in Clay Mineralogy, Chapman & Hall, New York (1987).
28. R.L. Frost, O.B. Locos, H. Ruan and J.T. Kloprogge, *Vib. Spectrosc.*, **27**, 1 (2001); J. Cornejo and M.C. Hermosin, *Clay Miner.*, **23**, 391 (1988).
29. S. Caillers and S. Henin, in ed.: G. Brow, Sepiolite, In The X-Ray Identification and Crystal Structure of Clay Minerals, The Mineralogical Society of London, Chap. 8, p. 325 (1961).
30. D.M. Moore and D.C. Reynold, X-Ray Diffraction and the Identification and Analysis of Clay Minerals, Oxford University Press: New York, edn 2, p. 378 (1997).
31. A. Singer, in eds.: J.B. Dixon and S.B. Weed, Palygorskate and Sepiolite Group Minerals, In: Minerals in Soil Environments, Soil Science Society of America: Madison, WI, USA, edn 2, p. 829 (1989).